HIGH ENERGY PROTON TRAPPING IN NEPTUNE'S ASYMMETRIC MAGNETOSPHERE

by

DREW TWEEDALE

A THESIS

Presented to the Department of Physics and Computer Science
and the Robert D. Clark Honors College
in partial fulfillment of the requirements for the degree of
Bachelor of Science

May 2025

An Abstract of the Thesis of

Drew Tweedale for the degree of Bachelor of Science
in the Department of Physics to be taken June

Title: Particle Trapping in Neptune's Asymmetric Magnetosphere

Approved: *Professor Carol Paty*
Primary Thesis Advisor

Neptune's magnetosphere shows significant deviations from the symmetric dipole structure observed at Earth, with higher-order multipole contributions creating an asymmetric and dynamic magnetic environment. This asymmetry may explain the unexpectedly weak proton radiation belts detected by Voyager 2, which fall well below the Kennel-Petschek limit. To investigate the role of magnetic field geometry in particle trapping, this thesis models the trajectories of high-energy protons (1–5 MeV) in Neptune's offset dipole field using the Boris integration method. By systematically varying the dipole offset (0–0.75 R_N), we analyze its impact on the equatorial loss cone width, a key factor determining particle stability in radiation belts. Results show that increased dipole offsets lead to broader loss cones at close radial distances, enhancing proton loss to Neptune's atmosphere, while at larger distances, stable trapping regions shift outward. These findings suggest that Neptune's asymmetric field structure could spatially sculpt the inner boundary of its radiation belts, potentially accounting for the localized depletion of high-energy protons observed during Voyager 2's flyby. The thesis underscores the need for future missions to resolve the interplay between multipole field contributions and magnetospheric dynamics at the ice giants.

Acknowledgements

I would first like to thank Carol Paty. She taught both my first and last class in the Clark Honors College, took me under her wing to do research during her sabbatical, instilled the importance of being a writer, and nurtured a passion for research. This thesis wouldn't have been possible without her. I also thank Jesse Wilson for his commitment while serving as the CHC Representative on my committee. Thank you to my friends, family, and friends who have become family; your support has been invaluable over the course of this project. This thesis is dedicated to my late mother and father, who both believed in the importance of education and hard work. You both shaped me into the person I am today, and I will love you always.

Table of Contents

List of Figures

List of Tables

Introduction

Neptune, the furthest planet in our solar system, had its first—and only—manmade visit by Voyager 2 during the summer of 1989 (Ness et al., 1989). In this brief flyby, we caught a glimpse of Neptune's eccentricities, ranging from an abnormal plasma population (Mauk, 2014) to peculiar magnetic field measurements (Ness et al., 1989). The latter perhaps might be the most atypical, with Neptune's field deviating far from what we're accustomed to with Earth's dipolar field. Neptune, along with Uranus, has a magnetic field that contains significant higher order spherical harmonic contributions, creating a strongly asymmetric and time varying field with respect to the solar wind direction (Paty & Arridge et al., 2020).

Earth's magnetic field, along with most planets in our solar system, can be well approximated by a magnetic dipole: a symmetrical field aligned closely with the axis of rotation, as shown in Figure 1. This dipole approximation sufficiently explains the trapping of high-energy particles in Earth's magnetosphere. This approximation, however, cannot be translated to Neptune, whose internal dynamo produces magnetic fields that require higher order contributions to replicate Voyager 2 measurements (Connerney et al., 1991). These contributions could significantly impact the way Neptune traps particles within its magnetic field, thereby impacting plasma populations observed by Voyager 2.

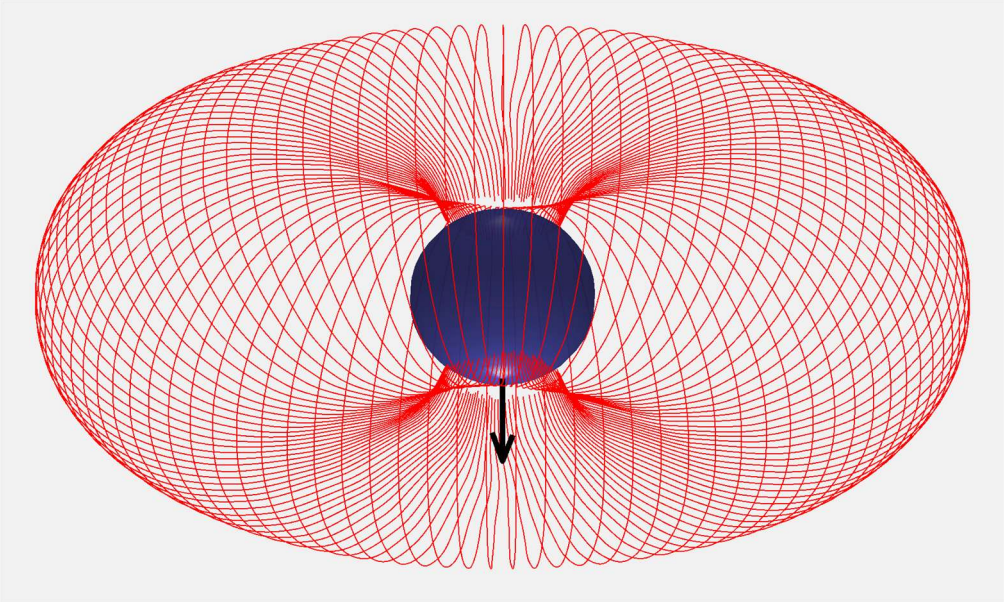

Figure 1: Planetary magnetic dipole

Visualization of a planet's magnetic dipole field. The black arrow signifies the direction of the dipole moment, and the direction of the magnetic field flows from the north to south pole.

The impetus for this thesis is an observation made by Voyager 2 during its stay in Neptune's magnetosphere: the relatively weak proton radiation belts—significantly below the Kennel-Petschek (KP) limit (Mauk, 2014). Interestingly, however, electron populations do approach the KP limit within the 1 MeV range (Mauk, 2014). The KP limit is the theoretical upper limit of particle density within radiation belts (Kennel C. F., & Petschek, 1966). Masters et al. (2022) hypothesized that the asymmetric structure of Uranus' field causes this discrepancy between electron and proton radiation belt populations. In a follow up study, Acevski et al. (2024) found that for 3 MeV particles (the highest energy Voyager 2 was able to detect), the dipole + quadrupole field shifted the particle's trajectory from the traditional dipole model. This shift was shown to account for the depleted high energy proton population within Uranus' inner magnetosphere, specifically where Voyager 2 made its flyby.

Voyager 2 also experienced an asymmetric cutoff in high energy proton flux during the period immediately after its closest approach at Neptune (Mauk et al., 1991). Uranus and

Neptune are alike in that they both have significant higher order field contributions, which begs the question: if Neptune and Uranus have similar magnetic field structures, would we expect Neptune's field to be responsible for the asymmetry in radiation belt population like the observed and modeled at Uranus? We aim to answer this question by taking a systematic approach to modeling asymmetric magnetic fields. A generalized approach is warranted, as both Uranus and Neptune are plagued by the lack of observational data.

This thesis will model the trajectory of charged particles using the Boris algorithm. Instead of using a dipole + quadrupole model to represent Neptune's field, we opted to use an offset dipole. We will simulate drift motions of high energy protons at finite distances around Neptune, showing that Neptune's asymmetric field can result in regions of high and low high energy proton population. This discrepancy would be an expected result of variations in the width of the loss cone as a function of dipole offset. Thus, Voyager 2 could have observed a region of lower particle density during its brief flyby, as the overall distribution of the particles could vary spatially due to the offset dipole.

Background

Planetary Magnetic Fields:

Planetary magnetic fields are often described as the gradient of a scalar potential. It's convenient to use a solution to this equation that represents the field as a sum of a series of potentials, with each separated into three coordinate variables. Since planets are spheres, it's natural to use spherical coordinates instead of cartesian multipoles due to the simplified geometry. Each term in the series represents a moment in the multipole expansion. Successive terms fall off by an additional power of 1/r, with r being the distance from the planet's center, as shown in Equation 1. The Schmidt Coefficients, g_n^m and h_n^m, also, on average, decrease rapidly for each successive multipole (Lowes, 1994). These two reasons are why the first term in the multipole expansion, the dipole, is often an effective approximation for the planetary magnetic field.

$$\Psi = R_N \sum_{\ell=1}^{\infty} \left(\frac{R_N}{r}\right)^{\ell+1} \sum_{m=0}^{\ell} P_\ell^m(cos\theta)(\mathrm{g}_\ell^m cos m\phi + \mathrm{h}_\ell^m cos m\phi) \quad (1)$$

On Neptune, however, Voyager 2 measured significant quadrupole and octupole field contributions, such that a simple dipole approximation was no longer valid at close planetary distances. To account for this, Neptune is typically modeled as an offset tilted dipole, where the dipole is "offset" from the center of the planet and "tilted" 47° westward from its axis of rotation, as shown in Figure 3 (Ness et al., 1989). By allowing the dipole to vary both in eccentricity and obliquity, the OTD model is able to effectively approximate the addition of higher order multipoles.

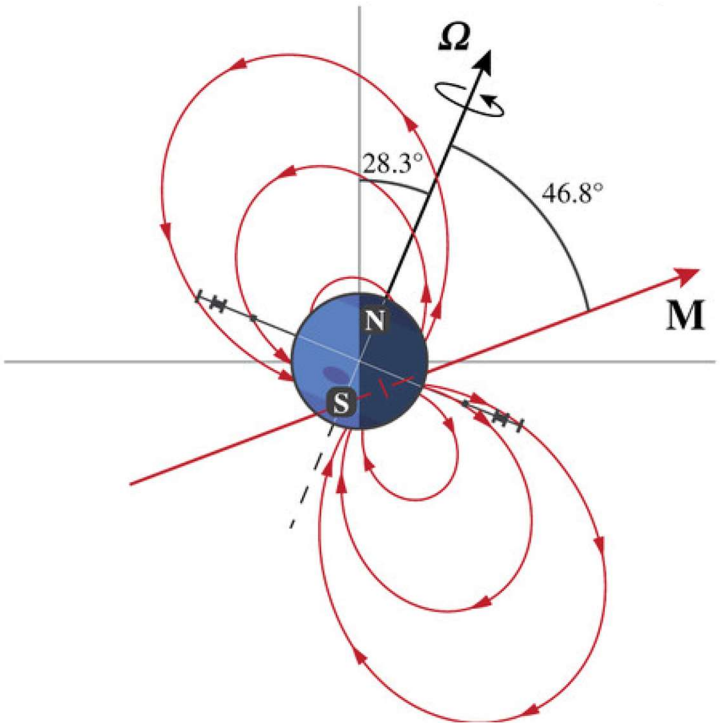

Figure 2: Offset tilted dipole model

2-D representation of Neptune's magnetic field modeled as an offset tilted dipole. **M** represents the dipole axis, and **Ω** represents the rotational axis. The white lines mapped over Neptune represent the rotational axis and equatorial plane, while the gray lines to the side Neptune represent the orbital plane. From "Ice giant magnetospheres", by Carol Paty and Chris S. Arridge et al., 2020, *Philosophical Transactions of the Royal Society of London. Series A: Mathematical, Physical, and Engineering Sciences*

It's important to note that not only is the OTD model an approximation used for mathematical convenience, but also that the location of the dipole bears no physical significance. The OTD model allows the dipole source to move from the planet's center, but this is merely an approximation to account for quadrupole and octupole field contributions. The location we wind up selecting for the eccentric dipole center is not related to Neptune's internal dynamo; it is merely the result of least-squares fitting (Lowes, 1994).

Neptune's eccentric magnetic field is most significantly influenced by the internal planetary dynamo (Connerney et al., 1991). On Earth, this dynamo is driven by currents

stemming from the movement of molten iron in the outer core. But on Neptune, this internal dynamo is thought to be attributed towards thin conductive shells residing at the bottom of Neptune's icy ocean close to the surface (Soderlund K. M., & Stanley S, 2020). The fact that the dynamo lies close to the surface influences the spatial distribution of the field, which could explain the higher order field contributions observed by Voyager 2.

Types of Magnetic Motion

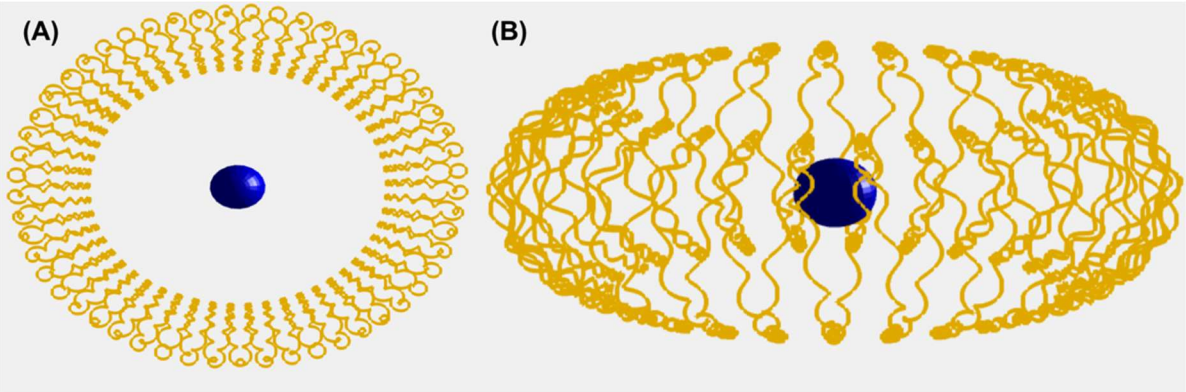

Figure 3: Particle motion in a dipole field

Simulation of a 1 MeV proton initialized 8 R_E from Earth's surface with a pitch angle of 35°. (A) shows the symmetry of mirror point latitudes resulting from the conservation of the first adiabatic invariant, and (B) shows the gyro, bounce, and drift motions for one full drift period.

Charged particles in the presence of a magnetic field experience an acceleration governed by the Lorentz force. Shown in Equation 2, a particle with charge q experiences a force proportional to the electric field strength $\vec{E}$, the magnetic field strength $\vec{B}$, and the velocity of the particle. The Lorentz force contains a cross product, which is an operation between two vectors—in this case $\vec{v}$ and $\vec{B}$—such that the resultant vector is perpendicular to both $\vec{v}$ and $\vec{B}$, with its direction dictated by the right-hand rule. In the absence of an electric field, a charged particle accelerates solely based on the magnetic field.

$$F = q\left(\vec{E} + \vec{v} \times \vec{B}\right) \tag{2}$$

Particle's influenced by a dipolar field experience three types of motion: gyromotion, bounce motion, and drift motion related to the first, second, and third adiabatic invariants, respectively. The extent of each motion varies due to a variety of factors, ranging from the charge, mass, or speed of the particle in question, to the strength of the magnetic and electric fields where the particle resides. Nonetheless, bounce, drift, and gyromotion all play a key role in the formation of radiation belts, sustaining magnetosphere currents, and governing plasma populations.

Gyromotion

Gyromotion refers to the circular motion of a moving charged particle around magnetic field lines as dictated by the Lorentz Force. The charged particle has a gyro-frequency—the time needed to complete one gyration—equal to T_g (Equation 3), and a gyro-radius equal to R_g (Equation 4). B is the strength of the magnetic field, while m and q are the mass and charge of the particle, respectively. The velocity, $v_\perp$, is the velocity component perpendicular to the local magnetic field vector.

$$T_g = \frac{2\pi m}{|q|B} \tag{3}$$

$$R_g = \frac{m v_\perp}{|q|B} \tag{4}$$

Bounce Motion

While gyromotion occurs if a particle is moving perpendicular to the magnetic field, bounce motion occurs if a particle is moving parallel to it (Baumjohann, 2022). In a dipole field, a particle will gyrate along the field lines until it reaches a mirror point: the point at which a particle reverses direction and travels towards the opposite pole. At this point, a particle's pitch

angle—the angle between a particle's velocity and local magnetic field vectors—reaches 90°, causing the particle to accelerate in the reverse direction. Its pitch angle gradually decreases until it reaches its equatorial pitch angle at the magnetic equator. Mirror points are a direct result of the conservation of the first adiabatic invariant, shown in Equation 5, and the resulting motion is called bounce motion.

$$\mu = \frac{mv_{\perp}}{2B} \tag{5}$$

During one full bounce motion, the second adiabatic invariant J, shown in Equation 6, is conserved. For the second adiabatic invariant, also called the longitudinal invariant, the particle's momentum is integrated along its trajectory, where s_1 and s_2 denote the location of the mirror points in opposite hemispheres. The conservation of J ensures that a trapped particle remains trapped in the planet's magnetic field as it completes a bounce orbit, so long as the magnetic field varies on timescales much longer than the bounce period.

$$J = \int_{s_1}^{s_2} \mathrm{mv}_{\parallel}\, \mathrm{ds} \tag{6}$$

Loss Cone

Even if the second adiabatic invariant is conserved, some particles still might not be trapped: if their mirror point lies deep within Neptune's atmosphere, or even beneath its surface, the particle will be lost due to collisions with neutral particles. A particle's equatorial pitch angle will determine the location of its mirror point. This lets us define an upper boundary—α_ℓ— such that any particle with an equatorial pitch angle smaller than α_ℓ is lost to Neptune's atmosphere. Such an angle, in three dimensions, carves out an equatorial loss cone in vector space that outlines whether a particle can successfully reach its mirror point, as shown in Figure 4.

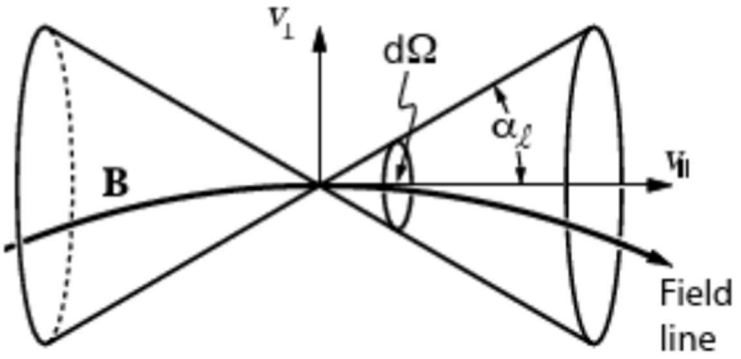

Figure 4: The loss cone

Diagram showing the loss cone carved out in vector space by the equatorial pitch angle α_ℓ. If a particle has an equatorial pitch angle less than α_ℓ (contained within dΩ), the particle will not mirror and will be lost in the planet's atmosphere. Diagram is from "Basic space plasma physics" (Third edition.), by Baumjohann W., & Treumann R. A. (2022). *World Scientific Publishing Company.*

The equation for the loss cone is shown in Equation 7. The loss cone depends solely on the particles L-value: the set of magnetic field lines that cross the magnetic equator at a given distance L (expressed in units of Neptune radii). It's worth noting that the loss-cone is defined for a dipole origin located at the planetary center. When this dipole center is offset, loss-cone width measurements will deviate from the predicted values. It's *especially* worth noting that the loss-cone is defined by the first adiabatic invariant, which is only the zeroth order term in an asymptotic series. For highly energetic particles, like the ones modeled in this paper, the higher order terms of the adiabatic invariant become significant. This leads to a modified loss cone, one that deviates from the curve described by Equation 7.

$$sin^2\alpha_\ell = (4L^6 - 3L^5)^{-1/2} \tag{7}$$

Drift Motion

As particles bounce between hemispheres and gyrate along field lines, they also drift around the planet. Particles will drift for a variety of reasons, ranging from inhomogeneity in the magnetic field to the curvature of magnetic field lines. In a simple dipole field, particles will experience a stronger magnetic force the closer they are to the magnetic pole, and a weaker field towards the magnetic equator. This difference causes a change in the size of a particle's gyro-radius (see Equation 3) over the course of its trajectory, causing an azimuthal shift in the particle's orbit.

Particles will also feel a centrifugal force that results from the curvature of magnetic field lines. This force is perpendicular to the magnetic field and its curvature and is proportional to the parallel particle energy. The associated drift, along with the drift stemming from the inhomogeneous magnetic field, pushes ions and electrons in opposite directions around the planet, thus creating a current called the ring current. This current is perpendicular to both the magnetic field and its curvature. This current creates its own magnetic field which, on Earth, plays an important role in protecting lower latitudes from magnetic storms (Roelof & Williams, 1988).

Magnetic drifts are held together by the third adiabatic invariant shown in Equation 8, which states that the magnetic flux encircled by the orbit of a charged particle trapped in an axisymmetric magnetic mirror is conserved. If the drift frequency is much larger than changes in the magnetic field, Φ is invariant and roughly equals the magnetic flux enclosed by the particle's orbit.

In Equation 5, M is the magnetic moment, v_d is the sum of all perpendicular drift velocities, ψ is the azimuthal angle, and the integration is taken along a full circular drift path of the particle.

$$\Phi = \oint v_d \, r d\psi = \frac{2\pi m}{q^2} M \tag{8}$$

Methodology

Standard particle motion is well understood in the context of a dipolar field, but the impact of higher order spherical harmonic field contributions on a particle's trajectory is relatively unknown. This thesis aims to model such a field at Neptune and show how a dipole's eccentricity impacts the trapping of high energy protons.

Boris Integration and the Offset Dipole Model

For particle simulations, we are using the Boris algorithm as it is the de facto method to advance a charged particle in an electromagnetic field. It also has the benefit of conserving phase space volume, which means that energy is conserved for the particle's orbit (Qin, 2013). It operates using a "leapfrog" method as a solution to the Lorentz equation, as it finds the position of a particle using the velocity a half time-step behind. Naturally, using finite time steps will introduce error in longer simulations. To address this, we minimized the simulation length to a maximum of one drift period and shortened the timestep to be 1/1000 of the gyro period. These changes, along with its ability to conserve energy, makes the Boris algorithm suitable to model orbital drift motions around Neptune. It's important to note that modifications must be made to the Boris method when particles reach relativistic speeds.

For out model, we used an offset dipole rather than an offset-tilted dipole. We want to explore the behavior of particles trapped in Neptune's field, but for a static field treatment the tilt of the field is arbitrary and does not affect the particle trajectories. Particles will move with respect to the magnetic field; the tilt of said field does not impact their trajectory; it only rotates the reference frame. Future work could seek to compare measurements obtained by Voyager 2 to our model's predictions, in which case the dipole tilt becomes relevant. In order to align Voyager

2 with our model at the time of Neptune's fly-by, the tilt of the magnetic dipole is paramount. This, however, is beyond the scope of this thesis.

The equations for dipole in cartesian coordinates are shown below:

$$B_x(x,y,z) = \frac{3B_0xz}{(r/R_N)^3r^2} \tag{9}$$

$$B_y = \frac{3B_0yz}{(r/R_N)^3r^2} \tag{10}$$

$$B_z(x,y,z) = \frac{3B_0(x^2+y^2-2z^2)}{(r/R_N)^3r^2} \tag{11}$$

The dipole moment, B_0 is given by the spherical harmonic model made by Connerney et al. (1991), and R_N is Neptune's radius. The equations are written in cartesian form due to its natural compliance with the Boris algorithm. The magnetic dipole is aligned with the z-axis, and the x-y plane represents the dipole's equatorial plane. The position vector, r, is measured from the origin, which is located at the center of the dipole.

Simulation Initialization

Protons were initialized with energies ranging from 1 to 5 MeV, as 5 MeV represents the upper limit of high energy particles Voyager 2 detected at Neptune (Krimigis, 1992). These protons were simulated sequentially at radial distances up to 8 RN from the dipole's center. Dipole offsets in the positive Z direction at were located a .25 R_N, .5 R_N, and .75 R_N. These offsets were chosen in part due to Neptune's eccentric dipole centered around .55 R_N from its planetary center (Connerney et al., 1991), but also to test the theoretical impact of even more extreme quadrupole and octupole field contributions.

This model neglects the effect of local electric fields which can heavily impact trajectories of low-energy plasma. Since magnetic motion scales with energy, however, electric field contributions are negligible when measuring high energy protons. Furthermore, the model neglects inter-particle interactions, which is reasonable since Voyager 2 measured relatively low high energy proton populations (Mauk, 2014). The simulation also neglects the temporal asymmetry inherent in Neptune's magnetosphere stemming from the tilt of the rotational axis. Depending on Neptune's rotation phase, the field can either have a pole-on or Earth-like orientation (Mejnertsen, 2016), yielding variable magnetic field interactions with the solar wind. This dynamic response of the magnetosphere is beyond the scope of this thesis.

The simulation begins by initializing a proton with a $0°$ pitch angle along the x-axis. The proton is then tracked until it collides with Neptune's atmosphere—a spherical boundary with a radius of 1 R_N shifted from the origin by the chosen offset—or is stably trapped. If the proton collides with Neptune, the simulation resets and the proton's pitch angle is increased by $1°$. This repeats until the proton is stably trapped. Once the proton is trapped, the simulation resets once again, but this time the pitch angle is decreased by one tenth of a degree. Finally, once the particle is lost once again, the particle's pitch angle is increased by one hundredth of a degree until the particle is stably trapped. This pitch angle is then recorded as the width of the equatorial loss cone. The simulation is repeated for each energy level and each radial distance.

Results and Discussion

The results of the simulation are shown below. Tables 1, 2, 3, and 4 show the equatorial loss cone measurements for dipole offsets of 0, 0.25 R_N, 0.5 R_N, and 0.75 R_N, respectively. Note that "…" is a placeholder for a particle that is stably trapped in Neptune's magnetic field. The L-shell value is the set of magnetic field lines that cross the magnetic equator at a given distance L (expressed in units of Neptune radii). The L-shells were measured from the origin of the coordinate system, while the offset simply shifted the boundary that represents Neptune's surface along the z-axis.

Loss Cone Width with Offset = 0 R_N,					
	Initialized Energy				
L-Shell (R_N,)	1 MeV	2 MeV	3 MeV	4 MeV	5 MeV
1.5	27.24°	27.25°	27.25°	27.25°	27.25°
2	16.33°	16.33°	16.33°	16.32°	16.32°
2.5	11.27°	11.26°	11.25°	11.25°	11.24°
3	8.38°	8.36°	8.34°	8.31°	8.29°
3.5	6.53°	6.47°	6.42°	6.36°	6.30°
4	5.22°	5.10°	4.97°	4.84°	4.71°
4.5	4.21°	3.96°	3.69°	3.40°	3.08°
5	3.34°	2.83°	2.20°	1.27°	…
5.5	2.46°	1.19°	…	…	…
6	1.27°	…	…	…	…
6.5	…	…	…	…	…
7	…	…	…	…	…
7.5	…	…	…	…	…

Table 1: Tabular data for high energy proton loss cone width for centered dipole.

Loss Cone Width with Offset = 0.25 R_N,					
	Initialized Energy				
L-Shell (R_N,)	1 MeV	2 MeV	3 MeV	4 MeV	5 MeV
1.5	33.14°	33.15°	33.15°	33.15°	33.15°
2	20.65°	20.65°	20.64°	20.64°	20.64°
2.5	14.56°	14.55°	14.54°	14.54°	14.53°
3	10.99°	10.97°	10.95°	10.94°	10.92°
3.5	8.66°	8.62°	8.58°	8.54°	8.49°
4	7.02°	6.93°	6.84°	6.75°	6.65°
4.5	5.78°	5.60°	5.41°	5.22°	5.02°
5	4.76°	4.42°	4.05°	3.63°	3.15°

5.5	3.85°	3.19°	2.34°	0.81°	…
6	2.90°	1.33°	…	…	…
6.5	1.65°	…	…	…	…
7	…	…	…	…	…
7.5	…	…	…	…	…

Table 2: Tabular data for high energy proton loss cone width for dipole offset of 0.25 R_N.

Loss Cone Width with Offset = 0.50 R_N,					
	Initialized Energy				
L-Shell (R_N,)	1 MeV	2 MeV	3 MeV	4 MeV	5 MeV
1.5	35.58°	35.58°	35.58°	35.58°	35.58°
2	23.46°	23.46°	23.46°	23.46°	23.46°
2.5	17.05°	17.05°	17.04°	17.04°	17.03°
3	13.13°	13.12°	13.11°	13.09°	13.08°
3.5	10.51°	10.48°	10.44°	10.41°	10.37°
4	8.63°	8.56°	8.48°	8.41°	8.33°
4.5	7.20°	7.06°	6.92°	6.77°	6.61°
5	6.05°	5.79°	5.51°	5.22°	4.90°
5.5	5.06°	4.58°	4.04°	3.40°	2.58°
6	4.11°	3.21°	1.88°	…	…
6.5	3.09°	0.55°	…	…	…
7	1.67°	…	…	…	…
7.5	…	…	…	…	…

Table 3: Tabular data for high energy proton loss cone width for dipole offset of 0.5 R_N.

Loss Cone Width with Offset = 0.75 R_N,					
	Initialized Energy				
L-Shell (R_N,)	1 MeV	2 MeV	3 MeV	4 MeV	5 MeV
1.5	34.76°	34.76°	34.76°	34.76°	34.76°
2	24.50°	24.50°	24.50°	24.50°	24.50°
2.5	18.50°	18.50°	18.49°	18.49°	18.49°
3	14.61°	14.60°	14.59°	14.58°	14.56°
3.5	11.91°	11.88°	11.85°	11.82°	11.79°
4	9.92°	9.86°	9.80°	9.73°	9.67°
4.5	8.39°	8.27°	8.15°	8.03°	7.90°
5	7.16°	6.94°	6.71°	6.47°	6.22°
5.5	6.10°	5.71°	5.29°	4.82°	4.29°
6	5.13°	4.44°	3.60°	2.46°	…
6.5	4.16°	2.84°	…	…	…
7	3.03°	…	…	…	…
7.5	1.19°	…	…	…	…

Table 4: Tabular data for high energy proton loss cone width for dipole offset of 0.75 R_N.

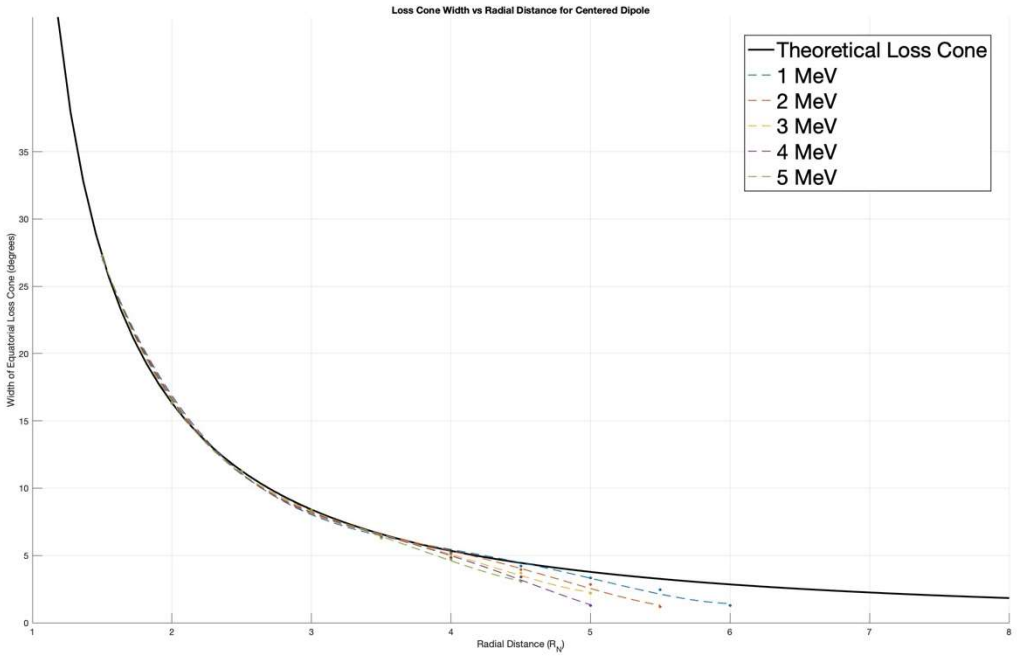

Figure 5: Loss cone width for centered dipole for protons between 1 and 5 MeV.

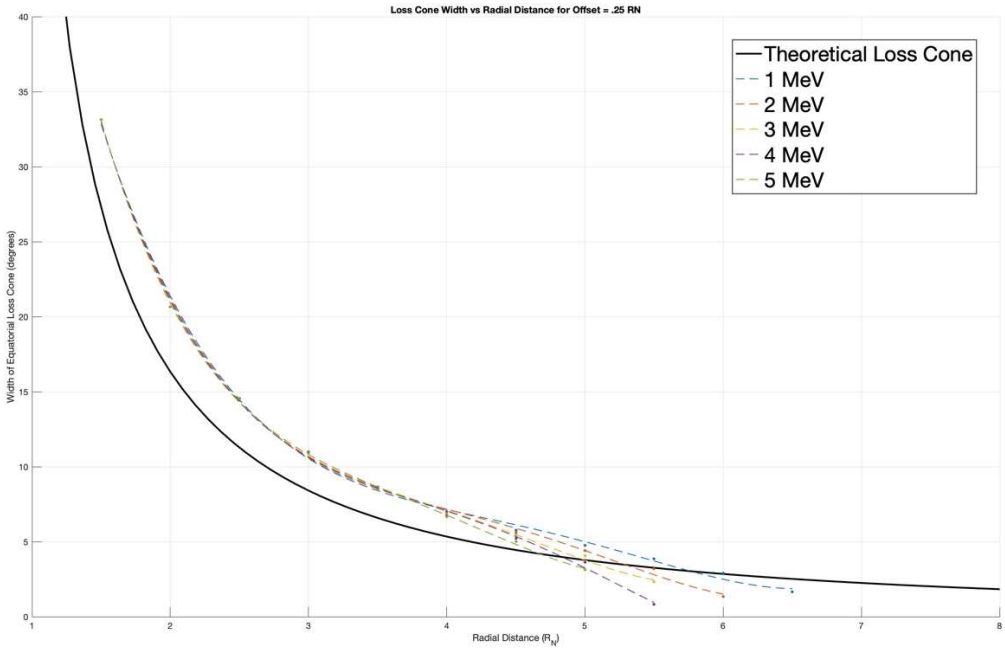

Figure 6: Loss cone width for dipole offset of 0.25 R_N for protons between 1 and 5 MeV.

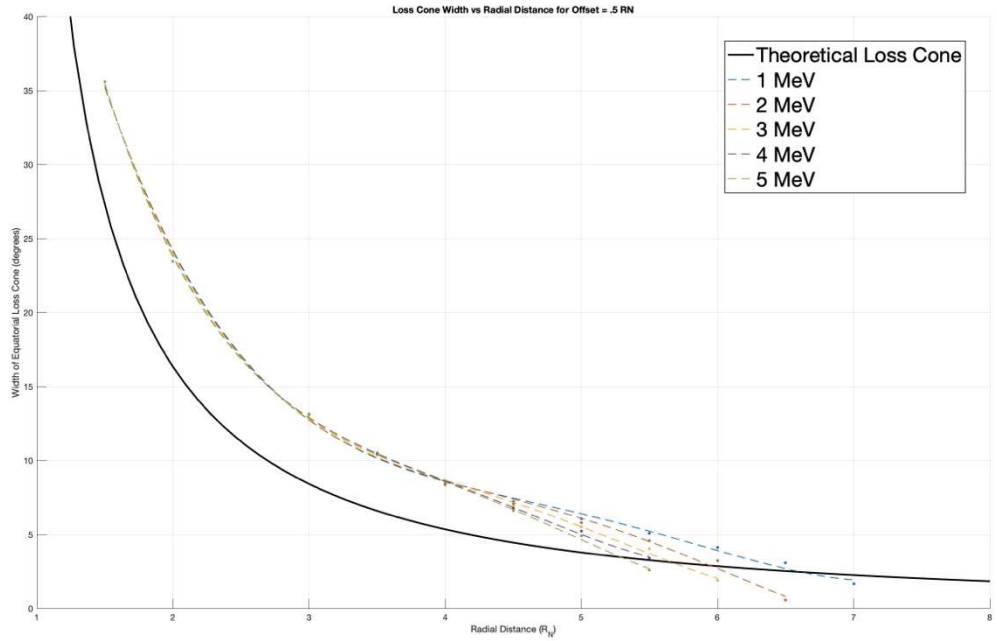

Figure 7: Loss cone width for dipole offset of 0.5 R_N for protons between 1 and 5 MeV.

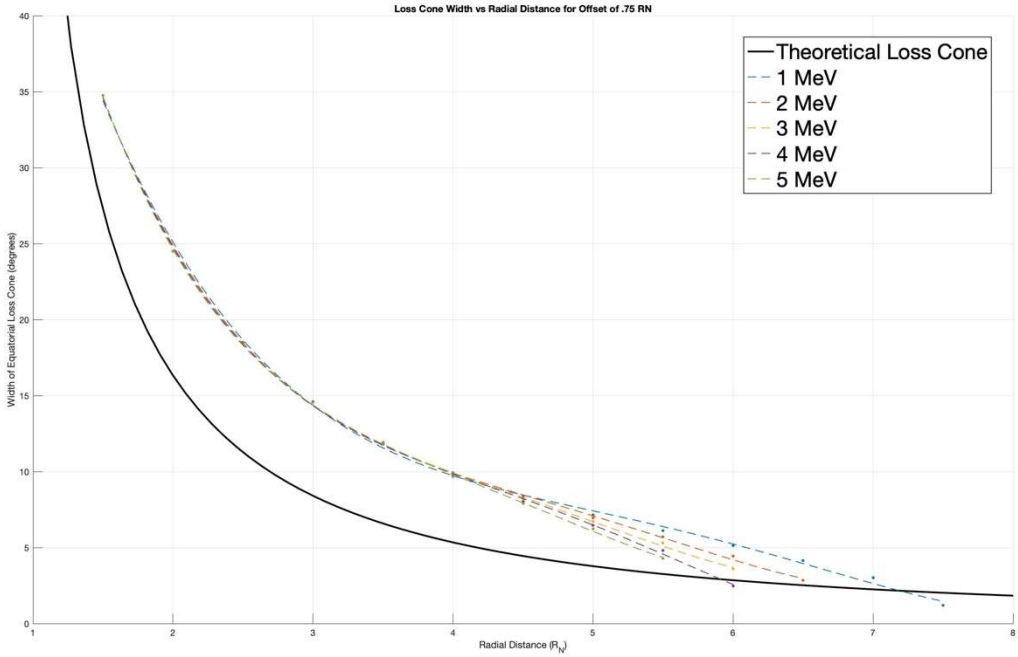

Figure 8: Loss cone width for dipole offset of 0.75 R_N for protons between 1 and 5 MeV

Graphical representations of the tabular data are shown in Figures 5, 6, 7, and 8, corresponding to dipole offsets of 0, 0.25 R_N, 0.5 R_N, and 0.75 R_N, respectively. The x-axes

display the radial distance from the center of the dipole, and the y-axes display the width of the loss cone, measured in degrees. The solid black line represents the idealized loss cone—the theoretical equatorial pitch angle boundary where particles above are stably trapped and particles below are lost to the atmosphere. The formula is defined in Equation 7. Note that the loss cone function on the figures is the same for each plot. This is due to the formula being defined for a centered dipole; Figure 5 illustrates this clearly, showing the data aligned most consistently with the theoretical prediction.

Loss cone width tended to increase as the dipole became more eccentric, with the most extreme shifts in magnitude seen at the closest L-shell values. For the L-shell of 1.5 R_N, the loss cone expanded from 27.45° at an offset of 0 R_N to 35.58° at an offset of 0.5 R_N. This makes sense, since a larger dipole offset results in particles colliding with Neptune's atmosphere that would otherwise bounce at high magnetic latitudes. Interestingly, the loss cone width decreased at an L-shell of 1.5 R_N between the offsets of 0.5 R_N and 0.75 R_N from 35.58° to 34.76°. This is due to the geometry of the system: for offsets larger than 0.5 R_N, protons close to Neptune would experience bounce motion beneath the planetary equator.

At further Neptune radii, an increased dipole offset corresponded with an increased radial distance for the boundary between lost and stably trapped protons. This is also likely due to the geometry of the system, as a positive dipole offset would decrease the amount of time a particle had to mirror, translating to a radiation belt that is shoved further from Neptune's origin. At these far radial distances, however, solar wind fluctuations would heavily influence a proton's trajectory, perhaps more so than the magnetic field given Neptune's rotational phase. For reference, Earth has two radiation belts: one that is between 1.1 and 3 R_E, while the other is concentrated between 4-5 R_E. The outer boundary, however, is extremely diffusive, and

sometimes extends outwards to around 10 R_E (Kilpua E. K. J., & Koskinen, 2021). Solar wind fluctuations are not accounted for in this simulation, so direct radiation belt location predictions cannot be made.

It's worth noting that the pitch angles for different energies at the same L-shell for the same offset were relatively constant for close radial distances but began to separate at further L-shells. This is likely due to the higher order terms of the first adiabatic invariant impacting the particle's trajectory. When particles with high energy levels in regions of low magnetic field strength, such as the magnetic equatorial regions at far L-shells, these higher order terms in the series become pronounced, especially when the pitch angle reaches 0° (Porazik et al., 2014).

For close L-shells where Neptune's internal magnetic field is strongest, the simulation shows that—assuming a uniform pitch angle distribution—more high energy ions will be stripped from Neptune's radiation belt as they collide with neutral particles in the atmosphere. These findings could explain the asymmetric drop off in high energy proton measurements observed in the period after Voyager 2's closest approach (Mauk et al., 1991), as the radiation belts could be sculpted by the eccentricity of the dipole—or the strength of higher order field contributions. At far radial distances, however, this model lacks generalizability, since it neglects temporal fluctuations from solar wind interactions and Neptune's rotational phase. But again, radiation belt location predictions are outside the scope of this model, since these are heavily dependent on the orientation of Neptune's field with respect to the solar wind.

Future Work

While this thesis explored the interaction between charged particles and an offset dipole, the next step would be making the model more Neptunian. To do so, we would need to model the magnetic field as a combination of higher order field contributions. One could approximate these contributions, while also being able to compare it to Voyager 2, through an offset *tilted* dipole. This would be an adequate approximation for the magnetic field beyond 4 RN, but closer in—Voyager 2's closest approach was within 1.18 RN—one must model explicitly the higher order multipole terms. Steps have been taken towards implementing a dipole + quadrupole magnetic field with Schmidt coefficients obtained from Connerney's spherical harmonic model (Connerney et al., 1991), but this work is beyond the scope of this thesis.

As stated in the discussion, to give accurate predictions about the specific location of Neptune's radiation belts, incorporating the temporal variance of Neptune's magnetosphere is a necessity. This would require modeling Neptune's rotation phase at the time of Voyager 2's flyby, as solar wind fluctuations interacting with Neptune's magnetic field orientation heavily influence the behavior of distant high energy particles. Implementing these modifications would allow us to compare our proton density predictions to Voyager 2's measurements. Ultimately, these measurements are merely a snapshot: future missions are needed to provide more insight on Neptune's highly dynamic magnetosphere.

Bibliography

Acevski, M., Masters, A., & Zomerdijk-Russell, S. (2024). Asymmetry in Uranus' High Energy Proton Radiation Belt. Geophysical Research Letters, 51(12). https://doi.org/10.1029/2024GL108961

Agre, M. Y. (2011). Multipole expansions in magnetostatics. Physics Uspekhi, 54(2), 167–180. https://doi.org/10.3367/UFNe.0181.201102d.0173

Baumjohann, W. (Wolfgang), & Treumann, R. A. (2022). Basic space plasma physics (Third edition.). World Scientific Publishing Company.

Borovsky, J. E., Yakymenko, K. N., & Delzanno, G. L. (2022). Modification of the Loss Cone for Energetic Particles in the Earth's Inner Magnetosphere. Journal of Geophysical Research. Space Physics, 127(8). https://doi.org/10.1029/2021JA030106

Connerney, J. E. P., Acuña, M. H., & Ness, N. F. (1991). The magnetic field of Neptune. Journal of Geophysical Research: Space Physics, 96(S01), 19023–19042. https://doi.org/10.1029/91JA01165

Connerney, J. E. P., Acuña, M. H., & Ness, N. F. (1987). The magnetic field of Uranus. Journal of Geophysical Research, 92(A13), 15329–15336. https://doi.org/10.1029/JA092iA13p15329

Kennel, C. F., & Petschek, H. E. (1966). Limit on stably trapped particle fluxes. Journal of Geophysical Research (1896-1977), 71(1), 1–28. https://doi.org/10.1029/JZ071i001p00001

Kilpua, E. K. J., & Koskinen, H. E. J. (2021). Radiation Belts and Their Environment. In Physics of Earth's Radiation Belts. Springer International Publishing AG.

Krimigis, S. M. (1992). Particles and fields measurements at Neptune with Voyager 2. Advances in Space Research, 12(11), 55–70. https://doi.org/10.1016/0273-1177(92)90423-U

Lowes, F. J. (1994), The geomagnetic eccentric dipole: facts and fallacies. Geophys. J. Int., 118, 671–679, https://doi.org/10.1111/j.1365-246X.1994.tb03992.x.

Masters, A., Ioannou, C., & Rayns, N. (2022). Does Uranus' asymmetric magnetic field produce a relatively weak proton radiation belt? Geophysical Research Letters, 49(23), e2022GL100921. https://doi.org/10.1029/2022GL100921

Mauk, B. H., Keath, E. P., Kane, M., Krimigis, M., Cheng, A. F., Acuna, M. H., Armstrong, T. P., & Ness, N. F. (1991). The magnetosphere of Neptune: Hot plasmas and energetic particles. Journal of Geophysical Research Supplement, 96(S01), 19061–19084. https://doi.org/10.1029/91JA01820

Mauk, B. H. (2014). Comparative investigation of the energetic ion spectra comprising the magnetospheric ring currents of the solar system. Journal of Geophysical Research: Space Physics, 119(12), 9729–9746. https://doi.org/10.1002/2014JA020392

Mejnertsen, L., Eastwood, J. P., Chittenden, J. P., & Masters, A. (2016). Global MHD simulations of Neptune's magnetosphere. Journal of Geophysical Research. Space Physics, 121(8), 7497–7513. https://doi.org/10.1002/2015JA022272

Ness, N. F., Acuña, M. H., Burlaga, L. F., John E. P. Connerney, Lepping, R. P., & Neubauer, F. M. (1989). Magnetic Fields at Neptune. Science (American Association for the Advancement of Science), 246(4936), 1473–1478. https://doi.org/10.1126/science.246.4936.1473

Paty, C., Arridge, C. S., Cohen, I. J., DiBraccio, G. A., Ebert, R. W., & Rymer, A. M. (2020). Ice giant magnetospheres. Philosophical Transactions of the Royal Society of London. Series A: Mathematical, Physical, and Engineering Sciences, 378(2187), 20190480–20190480. https://doi.org/10.1098/rsta.2019.0480

Porazik, P., Johnson, J. R., Kaganovich, I., & Sanchez, E. (2014). Modification of the loss cone for energetic particles. Geophysical Research Letters, 41(22), 8107–8113. https://doi.org/10.1002/2014GL061869

Qin, H., Zhang, S., Xiao, J., Liu, J., Sun, Y., & Tang, W. M. (2013). Why is Boris algorithm so good? Physics of Plasmas, 20(8), 084503. https://doi.org/10.1063/1.4818428

Roelof, E. C., & Williams, D. J. (1988). The terrestrial ring current - From in situ measurements to global images using energetic neutral atoms. Johns Hopkins APL Technical Digest, 9, 144–163.

Soderlund, K. M., & Stanley, S. (2020). The underexplored frontier of ice giant dynamos. Philosophical Transactions of the Royal Society of London. Series A: Mathematical, Physical, and Engineering Sciences, 378(2187), 20190479–20190479. https://doi.org/10.1098/rsta.2019.0479

Vogt, J., & Glassmeier, K. H. (2000). On the location of trapped particle populations in quadrupole magnetospheres. Journal of Geophysical Research, Washington, DC, 105(A6), 13063–13071. https://doi.org/10.1029/2000JA900006